The Andra Couplex 1 test case: comparisons between Finite-Element, Mixed Hybrid Finite Element and finite volume element discretizations

G. Bernard-Michel, C. Le Potier, A. Beccantini, Stephane Gounand, M. Chraibi

The Andra Couplex 1 Test Case : Comparisons Between Finite-Element, Mixed Hybrid Finite Element and Finite Volume Element Discretizations

G. Bernard-Michel (gilles.bernard-michel@cea.fr) and C. Le Potier (clepotier@cea.fr)
Commissariat à l'Énergie Atomique (CEA), DEN/DM2S/SFME/MTMS Saclay

A. Beccantini (alberto.beccantini@cea.fr) and S. Gounand (gounand@semt2.smts.cea.fr)
Commissariat à l'Énergie Atomique (CEA), DEN/DM2S/SFME/LTMF Saclay

M. Chrebi
Commissariat à l'Énergie Atomique (CEA), DEN/DM2S/SFME/MTMS Saclay

Abstract.

We present here results for the Andra Couplex 1 test case, obtained with the code Cast3m. This code is developped at the CEA (Commissariat l'nergie atomique) and is used mainly to solve problems of solid mechanics, fluid mechanics and heat transfers. Different types of discretization are available, among them finite element, finite volume and mixed hybrid finite element method. Cast3m is also a componant of the platteform Alliances (co-developped by Andra, CEA), which will be used by Andra for the safety calculation of an underground waste disposal in year 2004. We solve the Darcy equation for the water flow and a convection-diffusion transport equation for the Iodine 129 which escapes from a repository cave into the water. The water flow is calculated with a MHFE discretization. It is shown that this method provides sharp results even on relatively coarse grids. The convection-diffusion transport equation is discretized with FE, MHFE and FV methods. In our comparison, we point out the differences of these methods in term of accuracy, respect of the maximum principle and calculations cost. Neither the finite element nor the mixed hybrid finite element approach respects the maximum principle. This results in the presence of negative concentrations near the repository cave, whereas FV calculations respect the monotonicity. We show that mass lumping techniques suppress this problem but with strong restrictions on the grid. FE and MHFE approaches are more accurate than FV for the diffusion equation, but the overall results are equivalent since the advective terms are dominant in the far field and are discretized with centered schemes. We conclude by studying the influence of the grid: a very fine grid near the repository solves almost all the problems of monotonicity, without employing mass lumping techniques. We also observed a very important increase of the accuracy on a structured grid made up of rectangles.

Keywords: Couplex 1, convection-diffusion transport, monotonicity, finite volume, finite element, mixed hybrid finite element, grid influence

Abbreviations: FE – Finite Element; MHFE – Mixed Hybrid Finite Element; FV – Finite Volume

1. Introduction

We consider the ANDRA Couplex 1 test case [1], and more specifically the transport of the Iodine 129. It escapes from a repository cave into the water and its concentration is given by the convection-diffusion equation :

$$R\omega(\frac{\partial C}{\partial t} + \lambda C) - div(D\vec{\nabla}C + \vec{u}C) = s \quad \text{in } \Omega \times (0,T). \tag{1}$$

where Ω is an open bounded subset of $\mathcal{R}^2$, D is the diffusion/dispersion tensor, R the latency Retardation factor (equal to 1), $\lambda = \log 2/T_i$ with T_i being the half life of the element and ω the effective porosity.

The rock layers are saturated with water and boundary loads are stationary. The flow is therefore independent of time and Darcy's velocity u is given by Darcy's law :

$$u = -K\nabla h \quad \text{in } \Omega \times (0,T). \tag{2}$$

where K is the permeability tensor, assumed constant in each layer and h the dynamic load. All the coefficients are defined in [1].

The present paper is organized as follows. The numerical schemes are presented in Section 1. We describe the study of the space convergence in Section 2. We compare the accuracy of the different methods and their calculation cost in Section 3. Techniques of mass lumping, employed with FE and MHFE discretizations, are presented Section 4. A discussion Follows in Section 5.

2. Numerical schemes

2.1. MHFE for the flow

We calculate the flow $\vec{u} = -K\vec{\nabla}h$ with a mixed hybrid finite element method [2, 3]. Briefly, the method consists in solving the following problem :

$$\begin{cases} \vec{u} = K\vec{\nabla}h \\ div\vec{u} = 0 \end{cases} \tag{3}$$

The unknown h is discretized with functions which are constant on each cell, representing the average value of h. The flux is discretized in HDIV (L^2 norm of $\nabla.u$ is finite) for mixed finite element, whereas hybridization consists in introducing the trace of the unknown h on the boundaries of each cell to ensure the continuity of the flux across each cell. The problem is reformulated with the trace of head, as the only unknown variable.

2.2. FV for the transport equation

We choose a finite volume method described in [4, 5] for the diffusive part. For the convective part, we use a classical upwind scheme (order 1): the value of the concentration at one egde of a cell is the concentration at the center of the cell located on the upstream side of this edge. Let us give a few details about the first method. We are interested by the discretization of the operator $\nabla.(D\vec{\nabla}C)$ and we consider nearly the same problem as above, Eq. (3), with the diffusion tensor D instead of the permeability K, C the concentration of Iode 129, and the porosity ω multiplied by the retardation factor R before the time derivation:

$$\begin{cases} \vec{q} = D\vec{\nabla}C \\ R\omega\dfrac{\partial C}{\partial t} = div\vec{q} \end{cases} \tag{4}$$

2.2.1. *Notation*

We describe the method for a triangle for the simplicity of exposition. This method can be similarly extended to quadrangles (and even 3 dimensional elements). We use the following notation (Figure 1):

- S the triangle (P,Q,R) ; C,B and D the middles of its edges ; A its barycenter and A_S its area.
- T the triangle (A,B,C) ; δT its boundary and A_T its area.
- $\vec{n}_{AB}$, (and respectively $\vec{n}_{AC}$, $\vec{n}_{CB}$, $\vec{n}_{PB}$, $\vec{n}_{CP}$, $\vec{n}_{BQ}$, $\vec{n}_{DQ}$, $\vec{n}_{RD}$, $\vec{n}_{RC}$), a normal to $\vec{AB}$ (and respectively $\vec{AC}$, $\vec{CB}$, $\vec{PB}$, $\vec{CP}$, $\vec{BQ}$, $\vec{DQ}$, $\vec{RD}$, $\vec{RC}$) with the same length as this vector.
- Ω_p the quadrangular cell (A, B, C, P).
- N_P the number of edges of the mesh having the point P as endpoint.

2.2.2. *Algorithm*

We assume that C is affine on the quadrangular cell Ω_P, $\vec{q}$ is constant on Ω_P and D is constant on S. We denote by C_A (respectively C_B, C_C) the value of the function C at the point A (respectively B, C). Integration of the first equation of the system (4) over T, using Green's formula leads to :

$$\int_T D^{-1}\vec{q}d\Omega = \int_T \vec{\nabla}Cd\Omega = \int_{\delta T} C\vec{n}d\Gamma. \tag{5}$$

Using the assumption that C is affine on Ω_P, we get :

$$\vec{D}^{-1}q_P = \frac{1}{A_T}(C_A - C_C)\vec{n}_{AB} + \frac{1}{A_T}(C_A - C_B)\vec{n}_{AC}. \tag{6}$$

So, we deduce the flux f_{PB} through the interface BP as

$$f_{PB} = \vec{q}_P.\vec{n}_{PB} = \vec{n}_{PB}D\vec{n}_{AB}\frac{1}{A_T}(C_A - C_C) + \vec{n}_{PB}D\vec{n}_{AC}\frac{1}{A_T}(C_A - C_B). \tag{7}$$

Applying the flux continuity condition on each edge having P as a vertex, we deduce the interface value (C_B, C_C, etc...) by inverting a small matrix of dimension N_P. Then, we can reconstruct all the fluxes around the point P. Let us integrate the mass conservation equation (the second equation of the system 3) over a cell S. We get:

$$\begin{aligned} \int_S R\omega\frac{\partial C}{\partial t}d\Omega &= \int_S div\vec{q}d\Omega & (8)\\ &= \int_{\delta S}\vec{q}.\vec{n}d\Gamma & (9)\\ &= f_{PB} + f_{BQ} + f_{QD} + f_{DR} + f_{RC} + f_{CP}; & (10) \end{aligned}$$

that is to say:

$$A_S R_S \omega_S \frac{\partial C_A}{\partial t} = f_{PB} + f_{BQ} + f_{QD} + f_{DR} + f_{RC} + f_{CP}. \tag{11}$$

So, we are able to calculate the value C located at the barycenter of each cell of the grid. Indeed, once the time discretisation is done (we use Euler implicit, Explicit and Cranck-Nicholson scheme), the equation is discretized as a linear expression of the concentration at the center of each cell of the grid. The matrix of discretization is not symetrical.

2.2.3. *Properties of the algorithm*
The scheme seems to be consistent on triangular and quadrangular cells using the usual L^2 norm. It is conservative. It is monotone if the grid is regular enough. Unfortunately, we know that this algorithm can be unstable using very distorted cells and anisotropic tensors.

2.3. MHFE for the transport equation

2.3.1. *Algorithm*
The diffusive term is discretized like the flow equation. The advective term's discretization is similar to a finite volume approach. The $div(uC)$ term is integrated on each cell. The volume integral is then changed into a boundary integral where appears the convective flux

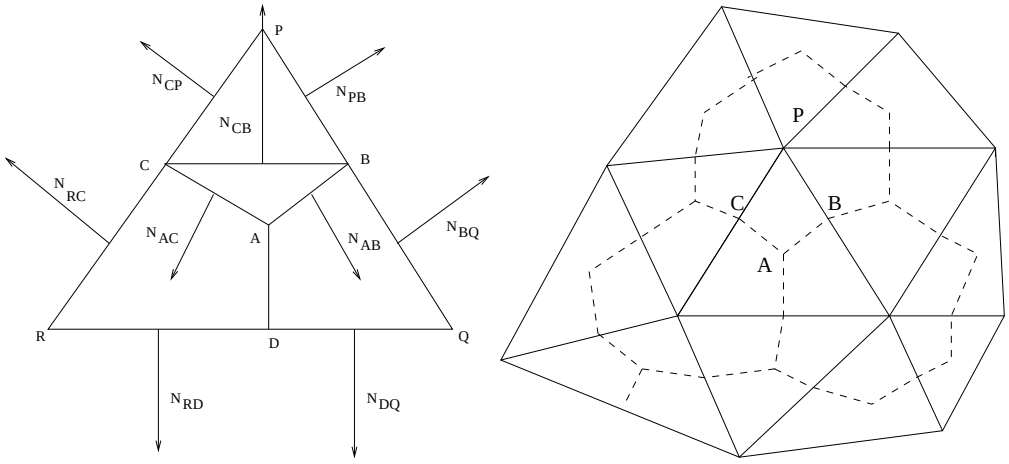

Figure 1. Case of triangular cells

$uC.n$. This flux is calculated using the trace of the concentration and the velocity flux, available with the MHFE method [6]. This is an order two discretization. Similar techniques could have been employed [7, 8], but we wanted to avoid a splitting between convection and diffusion discretization, as it is the case in Siegel *et al.*. Our technique allows a fully implicit scheme, by the use of Mixed Hybrid Finite Element for both the diffusive and the convective terms. On the other hand, the convection scheme does not respect the monotonicity. Whenever the Peclet number is higher than 2, we add some orthotropic numerical diffusion.

We also tried a splitting algorithm using a finite volume scheme for convection and a Mixed Hybrid Finite Element scheme for diffusion.

2.3.2. *Properties of the algorithm*

The scheme is consistent on triangular and quadrangular cells using the usual L^2 norm. It is conservative. It is monotone if the cells Fourier number $Fo_i = D\Delta t/d_i$ is larger than 1/6, where Δt is the time step and d_i the typical size of the cell along the i^{th} axis. The concentration and the fluxes are approximated with the same accuracy $O(d)$, where d is a typical cell's dimension.

The cell Fourier number is higher than 1/6 whenever the concentration diffuses beyond one sixth of a cell during a time step. The cells have therefore to be small enough, or the time steps large enough. This can't be easily achieved when the time step is controlled by other phenomena (coupling problems or presence of short period source terms).

2.4. FE for the transport equation

We use a standard Galerkin, linear (or bilinear on quadrangles) discretization. The scheme is consistent on triangular and quadrangular cells using the usual L^2 norm. It is not locally conservative, but is conservative on the domain. It is not monotone. The concentration is accurate as $O(d^2)$ and the fluxes are accurate as $O(d)$, for the L^2 norm. We have also made a calculation, with a quadratic FE method, providing accuracy of $O(d^3)$ for the concentration.

2.5. Time discretization

Let us denote AC the space dicretization of the diffusion operator $\nabla.(D\vec{\nabla}C)$, BC the space discretization of the convection operator $\nabla.(\vec{u}C)$, and IdC the discretisation of C. We use an implicit method. Therefore, the scheme writes, at a given time step n :

$$\begin{cases} R\omega Id(\dfrac{G^{n+1}-G^n}{\Delta t}) - AG^{n+1} + BG^{n+1} = S^n e^{\lambda t^n} \\ C^{n+1} = G^{n+1} e^{-\lambda t^{n+1}} \\ G^0 = C^0 \end{cases} \tag{12}$$

where Δt the time step, $t^n = n * \Delta t$, and G^n is introduced as a change of variable to solve analytically the decaying term $R\omega\lambda C$. Of course, this scheme is unconditionnaly stable.

The source term, from the Couplex 1 data file, is time integrated. Then, for each time step, the discretized source term is calculated as the difference between the integrated source at the end and at the beginning of the time step.

The change of variable makesit possible to solve analytically the radioactive decaying term of the equation.

2.6. The solvers used

The calculations were run on 1.7 GHz PC with 500 Mb of RAM memory. At each time step, we solve a linear sparse system which is not symmetric due to the convection operator. For the smallest grids (less than 50000 nodes), we use a direct solver. For larger numbers of nodes, we use a BCGSTAB algorithm and a ILU(0) preconditioning. This enables us to load only non-zero coefficients of the matrix discretization. The nodes were renumbered in all cases with the algorithm of Gibbs-King [9] to minimize the profile. It is essential for direct method but also very efficient for the iterative method. It indeed allowed a gain of at least a factor 3 in the number of iterations during the calculations.

2.7. The grid

Two sets of grids were used. The first one follows exactly the different layers and is made up of quadrangles. The second set does not exactly follow the inclined boundary of the repository's layer. It is made up of rectangles; therefore, the layer's boundary is a broken line. The first and second types of grid are very similar, except that the angles are around 90 ± 2 degrees for the first one.

The two approaches lead to the same results concerning the contour levels of iodine 129. Nevertheless, the velocity profiles at x=50, 12500 and 20000m are wrong up to a factor 2 for the vertical component, in the case of a rectangular mesh. This is a purely local effect, which is observed only with certain grids, where the observation lines are close to a jump of the repository layer's boundary (constituted with a broken line). It has very little negative effect on the final results on the iodine concentration. On the contrary, we will show that a better convergence is achieved on the rectangles with the three methods presented here.

2.8. The contour level lines

For the concentration, the contour level are drawn for the concentrations 10^{-12} (symbol A), 10^{-10} (B), 10^{-8} (C), 10^{-6} (D) and 10^{-4} (E).

We first encountered problems with the plotting software, which works in simple precision and was calculating wrong contour levels. The problem has been solved by segregating the values above or below the chosen levels (in double precision). The contour levels are then plotted, but without any interpolation, that is to say they follow the edges of the meshes.

3. Convergence Analysis

We use two different sets of five different grids, one set containing grids made up of rectangles, GRi, $i = 1,...,5$, and the other containing grids made up of quadrangles, GQi, $i = 1,...,5$. The coarsest ones, GQ1 and GR1, consist of 5000 cells; the second ones, GQ2 and GR2, of about 26000 cells; GQ3 and GR3, of about 55000 cells; GQ4 and GR4, of 88000 cells, and GQ5 and GR5 of 166000 cells. We point out that the number of unknowns is equal to the number of vertices for the FE method and to the number of cells for the FV method. These are roughly the same for the type of grids considered here. However, the number of unknowns for the MHFE method is equal to the number of

edges, nearly double the number of unknows needed for the other two methods.

3.1. The flow equation

Calculation for the flow equation using the mixed hybrid method with the grid GQ5 gave results nearly identical to those obtained with the grid GQ1. This indicates that a small number of cells is sufficient. The contour level curves for the piezomztric head are presented in Figure 2. In Figures 3, 4 and 5 are shown the Darcy velocity fields along the vertical lines $x = 50m$, $x = 12500m$, and $x = 20000m$, respectively.

3.2. The transport equation - Spatial convergence

The tests of spatial convergence were performed with small enough time steps so that time discretization errors were negligible. We used 100 year time steps from 1000 up to 2000 years, 250 year time steps from 2000 to 10110 years, 500 year time steps from 10110 to 50110 years, 2500 year time steps from 50110 to 2×10^5 years, 5000 year time steps from 2×10^5 to 10^6 years and 10000 year time steps from 10^6 to 10^7 years. To check that this list was satisfactory, we compared results obtained using three different time stepping schemes, Euler implicit (first order), Crank-Nicholson (second order), and an explicit scheme.

In Figures 6, 7, 8, 9, and 10 we show level curves of the concentration at 200000 years, and in Figures 11 and 12 at 10^6 years. Except where otherwise noted, a centered scheme for the advective term was coupled with the specified scheme for the diffusive term and an implicit scheme was used for the time stepping.

We observe that the calculations are not fully converged, even with more than a hundred thousand nodes, see Figures 6, 7, 11 and 12. For example, in Figures 11 and 12, when the calculations are carried out using the grid G2, the contour level D is located mostly in the clay layer. However, when the grid G4 or G5 is used the corresponding contour level is located almost entirely in the bottom layer. In Figures 6, 7, and 9, the contour level in the limestone layer, that exits from and re-enters the clay layer, decreases in size as the grid is refined.

We point out that all of the methods studied perform better on the grids of rectangles than on the grids of quadrilaterals see Figures 8, 9, and 10. The results obtained with either of the three methods, FE, FV, or MHFE, on the grid GR4 made up of rectangles show less diffusion than those obtained with the FE method on the finer grid GQ5 made up of quadrangles. Generally speaking, with each of the methods considered here, we obtain results of the same quality on the grid GR2 made up of rectangles as on the finer grid GQ4 and GQ5 made up of

quadrilaterals. (We can not really talk about superconvergence here as we haven't calculated errors and rates of convergence).

We also point out that upwind schemes are far less accurate than centered ones, as illustrated Figure 7. To complete this section, we present selected results obtained by the different methods tested at the remaining years 10110, 50110 and 10000000, in Figures 13 and 14.

4. Comparison of the different methods

4.1. Accuracy

The previously exposed results, Figures 8 and 9, show that MHFE compares well to the FE methods for a same grid. The same conclusion applies to the FV discretization, see Figures 6 and 10. However, we have compared the FV and MHFE methods on a simple diffusion equation with analytical solution. Both methods were converging at the same rate, but the constant of error was three times less important for the MHFE discretization. It seems therefore that MHFE are more accurate for the diffusion term. In the present problem, most of the comparisons are done outside the clay layer, where advection dominates. This might partly explain why the higher accuracy of the MHFE method is not observed.

4.2. Calculation cost

For the considered grids, we checked that the finite volume and the finite element discretization generate sparse matrices, the size of which is 9 times the number of unknowns, whereas the MHFE produce a matrix, the size of which is 7 times the number of unknowns. However, the calculation cost of the different methods is difficult to evaluate. On the average, we observed that the calculation costs for all three methods were almost the same, for the same number of unknowns (but we remind that there are twice as many unknowns for the EFMH discretization than for FE or FV discretizations on a same grid).

However, it has to be noticed that the MHFE method happened to be far slower when the mesh was strongly distorted. It seemed to be a lot more sensitive to the quality of the grid than the other methods. The number of iterations required by the BiCGSTAB algorithm to converge could be 10 times higher on a bad quality grid. The memory load is also very similar between the different methods with a slight advantage to the MHFE discretization.

Nevertheless, the presented results show that MHFE method requires a grid just as highly refined as the other two methods, in order to

math their accuracy, for this particular COUPLEX 1 problem. Therefore, the MHFE method is more expensive, since it requires twice as many unknowns than the two others methods presented. This contradicts what we said in Subsection 4.1, where the EFMH was said to be tree time more accurate than the FV method on a diffusion problem, for the same grid. We carried out other comparisons, on different types of grids (triangular, rectangular ...) and different types of equations. It shows that the accuracy of the different methods depends strongly on the grid and the equation. No general rule could be found concerning their accuracy; the MHFE discretization is sometimes much more accurate (3 or 4 times) than the FE or FV discretization, but it might also be the opposite.

On a pentium 4, 1,7 Ghz and 500 Mo of memory, for the G4 grid, it takes between 1 second (with 12 iterations) and 4.5 seconds (for 60 iterations) to solve a time step with a BiCGSTAB algorithm. The numerotation of the grid proved to be very important, even for an iterative method. It takes about 12 seconds to solve a time step with a direct method and then 0.3 second to solve each following time step, for an identical time increment.

On such a two-dimensional problem, a direct solver seems to be more appropriate and leads to calculations of less than 12 minutes on grid 4 for 1173 time steps for the FE discretization.

5. The maximum principle

Neither the FE nor the MHFE discretization of the transport equation preserves the monotonicity. When the concentration is rapidly varying, as is the case at early times near the repository, the calculated concentration shows oscillations, Figure 15.

When diffusion is dominant, i.e. the cell's Peclet number is smaller than 1, these oscillations are suppressed whenever the Fourier number is high enough. This can be achieved by reducing the cells size or by increasing the size of the time step, see Figure 13. However, it is not always possible to choose a larger time step or a finer grid. An alternative is to use a mass lumping technique. For an FE discretization, this consists in creating a diagonal time discretization matrix dC/dt by summing the terms of each row of the matrix and putting the sum in the diagonal slot. For the MHFE discretization, the technique is the same but with the mass matrix of the flux equation $q = -D\nabla C$.

This technique suffers strong restrictions. It can be employed only with rectangle cells for the MHFE, or with Delaunay-Voronoi meshes (for isotropic diffusion tensor). In this second case, the technique is

more complicated than a simple sum. For the FE method, it works only with Delaunay-Voronoi meshes (for isotropic diffusion tensor).

When the diffusion is negligible compared to the advective term (Peclet larger than 1), problems of monotonicity are reduced by adding numerical diffusion along the flow lines, in order to reduce the Peclet number down to 1. We are speaking of an upwind scheme in this case, and a centered scheme otherwise.

Practically, the mass lumping proved to be efficient with the MHFE method but rather inefficient with the FE discretization, Figure 16. Indeed, the mass lumping technique has been used on quadrangles (for the FE method) or non Delaunay-Voronoi triangles, and leads to worse results than those presented in Section 3.2. These bad results are mainly due to the presence of a centered convective term. When it is removed, the results are indeed free of oscillations. The use of Stream Upwind Petrov Galerkin scheme will be the object of a future work.

6. Discussions

The three methods studied here lead to results of similar quality. Whenever respecting monotonicity is important, the FV approach is more efficient than the FE or the MHFE technique. Indeed, mass lumping and upwind techniques work under strong restrictions. The other alternative, consisting in using fine grids also poses problems, particularly for problems in 3 dimensions.

Nevertheless it is possible to employ other techniques to ensure the positivity of the results. We envisage to work on the $\log(C)$ variable. We could benefit from the superior flexibility of FE and MHFE method, whose consistency is proved, even for very distorted meshes.

We envisage to use a second order FV scheme for the advective term and a SUPGDC upwind technique for the FE algorithm [10], which is a non linear discontinuity capturing method inducing numerical diffusion along the flow lines, and also along the gradient of the concentration.

A splitting algorithm using a MHFE discretization for the diffusion and a FV discretization for the advection has been tested. It works well, but requires small time steps (nearly as small as those required by a time explicit scheme). We are working on improving this technique.

References

1. "Couplex1 Test Case, Nuclear Waste Disposal Far Field Simulation", (2001)

2. Fraejis de Veubeke X.B. "Displacement and equilibrium models in the finite element method", in Stress Analysis, O. C. Zienkiewicz ang G. Hollister, eds. John Wiley & Sons, New York, NY, 1965.
3. ARNOLD D.N. and BREZZI F. "Mixed and nonconforming finite element methods: implementation, post processing and error estimates", R.A.I.R.O, Model. Math. Anal Numer., Vol. 19, pp. 7-32, 1985.
4. AAVATSMARK I., BARKVE T., BOE O., MANNSETH "Discretization on unstructured grids for inhomogeneous, anisotropic media. Part I: Derivation of the methods", Siam J. Sci. Comput., Vol. 19, num. 5, pp. 1700-1716, September 1998
5. AAVATSMARK I., BARKVE T., BOE O., MANNSETH "Discretization on unstructured grids for inhomogeneous, anisotropic media. Part II: Discussion and numerical results", Siam J. Sci. Comput., Vol. 19, num. 5, pp. 1717-1736, September 1998
6. DABBENE F. "Schémas de diffusion-convection en éléments finis mixtes hybrides', Rapport CEA DMT/95/613, Saclay, 1995.
7. SIEGEL P., MOSÉ R., ACKERER Ph. "Solution of the advection-diffusion equation using a combination of discontinuous and mixed finite elements", International Journal For Numerical Methods in Fluids, 24, pp. 595-613, 1997.
8. CHAVENT G. and JAFFRÉ J. "Mathematical models and finite elements for reservoir simulation", North Holland, Amsterdam, 1986.
9. LEWIS J.G. "Implementation of the Gibbs-Poole-Stockmeyer and Gibbs-King algorithms", ACM Trans. Math. Software, Vol. 8, pp. 180-189, 1982.
10. HUGHES T.J.R., MALLET M., MIZUKAMI A. "A new finite element formulation for computational fluid dynamics: II. Beyond SUPG", Computer methods in applied mechanics and engineering, Vol. 54, pp. 341-355, 1986.

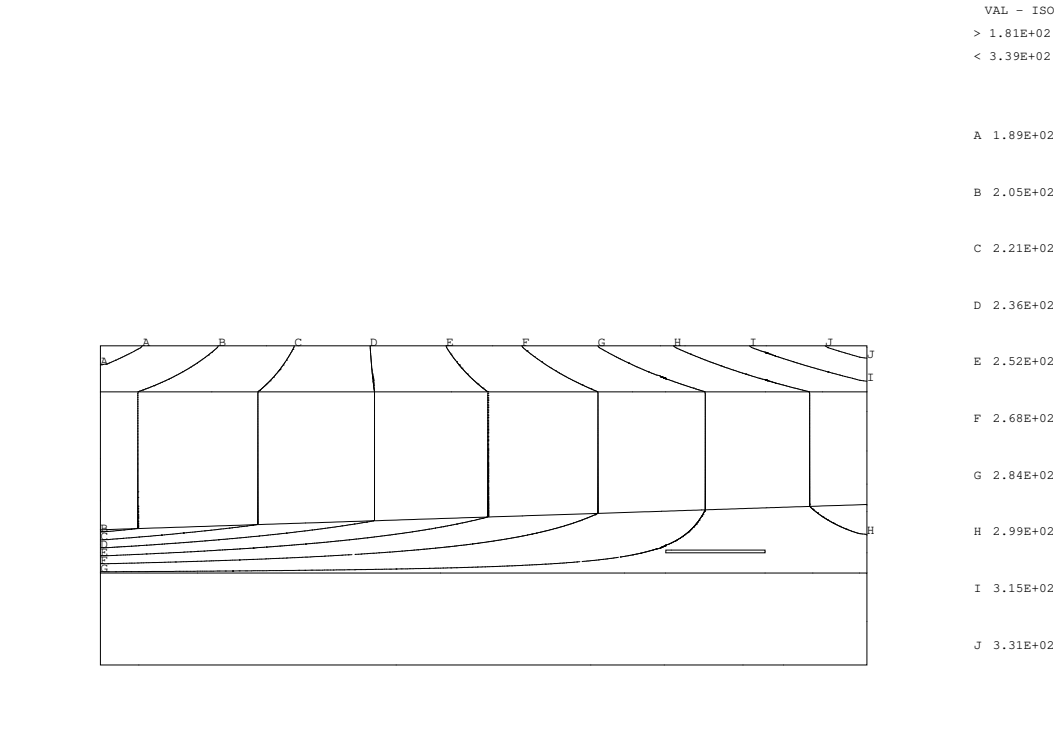

Figure 2. Isovalues of the piezometric head, MHFE, grid 1

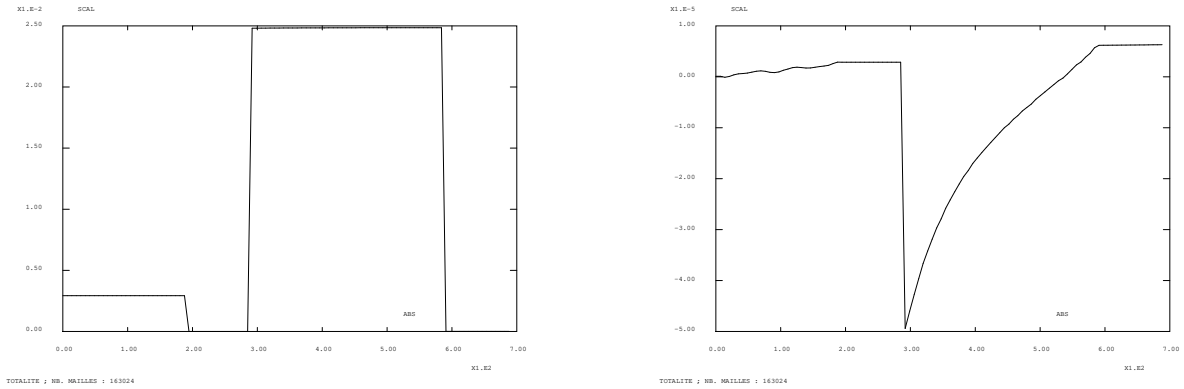

Figure 3. Darcy velocity field (u_x, u_y) at x = 50m, GQ5 grid, 332000 unknowns

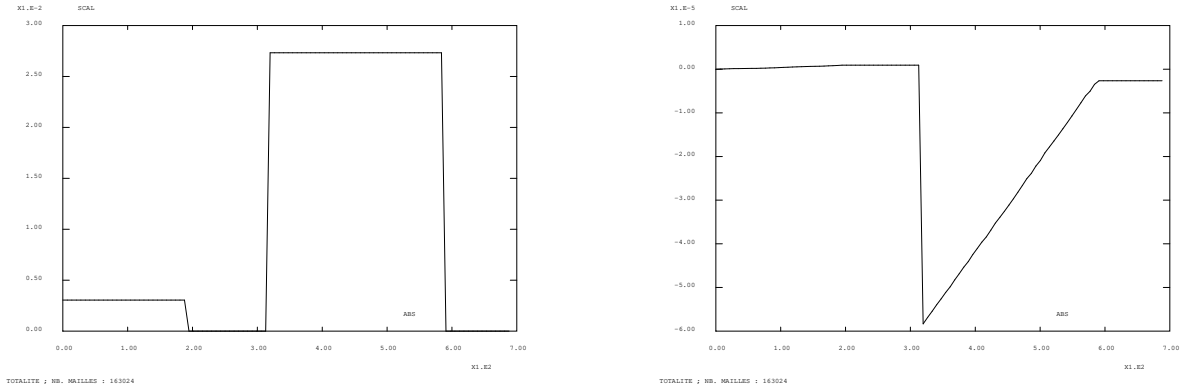

Figure 4. Darcy velocity field (u_x, u_y) at x = 12500m, GQ5 grid, 332000 unknowns

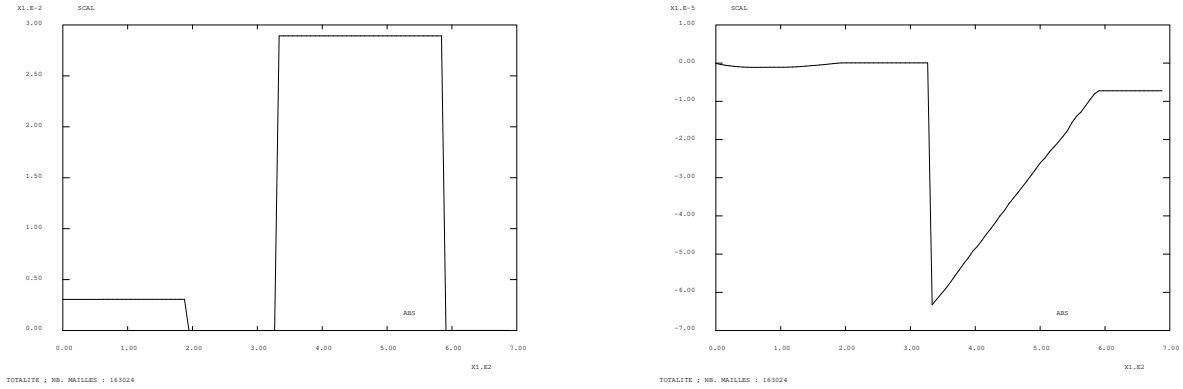

Figure 5. Darcy velocity field (u_x, u_y) at x = 20000m, GQ5 grid, 332000 unknowns

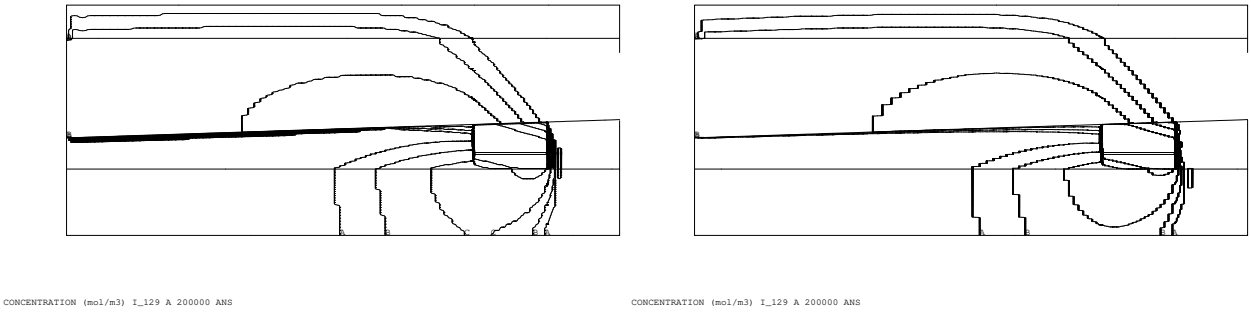

Figure 6. Results at 200000 years, grids GQ2 and GQ3 - quadrangles - FE discretization - centered advection

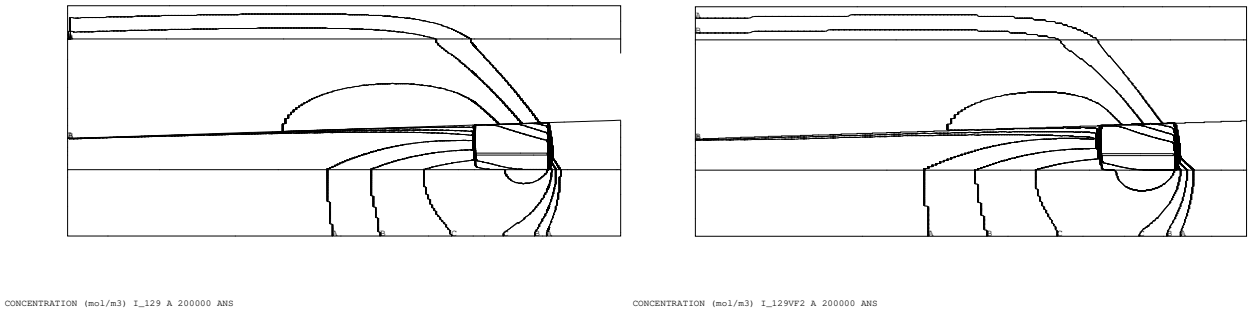

Figure 7. Results at 200000 years, grid GQ5 - quadrangles - with an FE discretization - centered advection and G4 - rectangles - with an upwind FV discretization

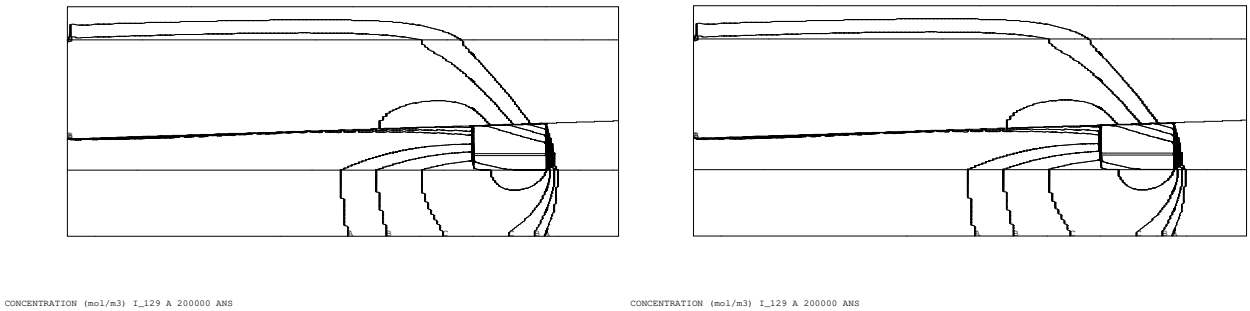

Figure 8. Results at 200000 years, grid GR4 - rectangles - with a bilinear FE discretization and grid GR2 - rectangles - with a quadratic FE discretization (centered advection for both)

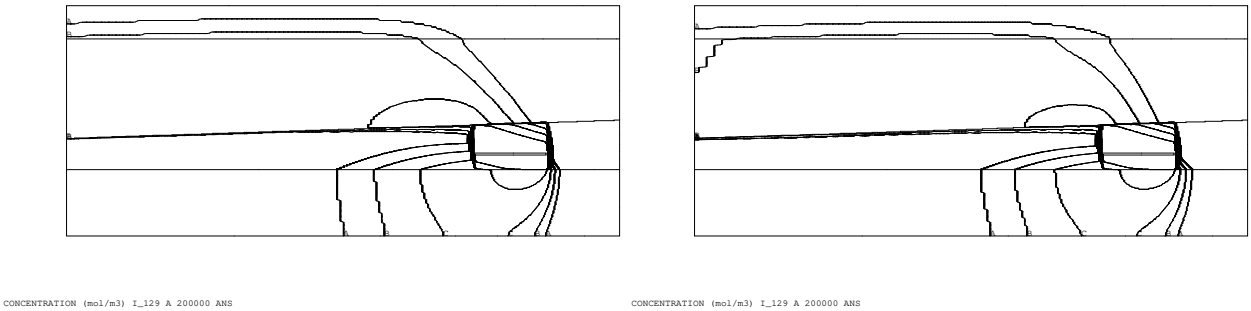

Figure 9. Results at 200000 years, grid GR4 - rectangles - MHFE discretization (left), splitting method - MHFE for diffusion - centered FV advection (right)

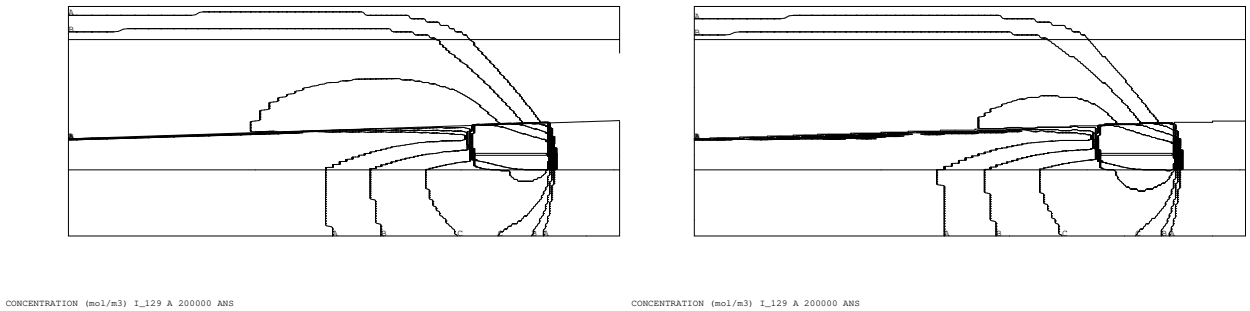

Figure 10. Results at 200000 years, grids GQ2 - quadrangles (left) and GR2 - rectangles (right) - FV discretization - centered advection

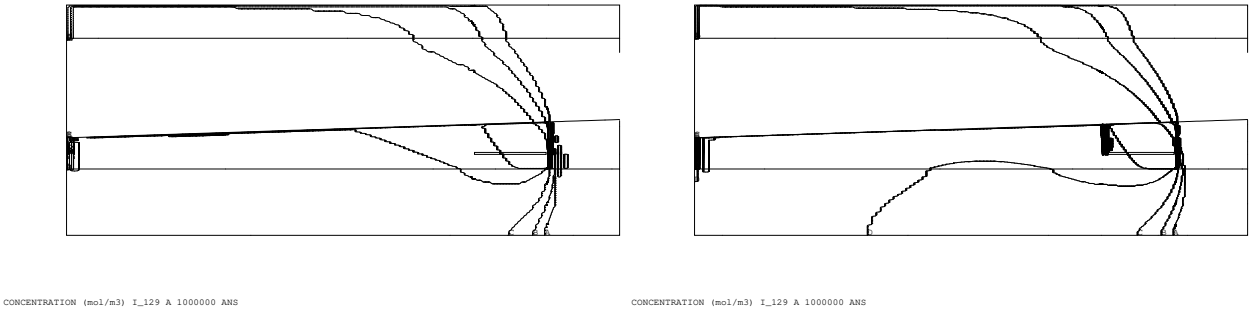

Figure 11. Results at 1000000 years, grids GQ2 and GQ4, FE discretization, presence of small oscillations - quadrangles

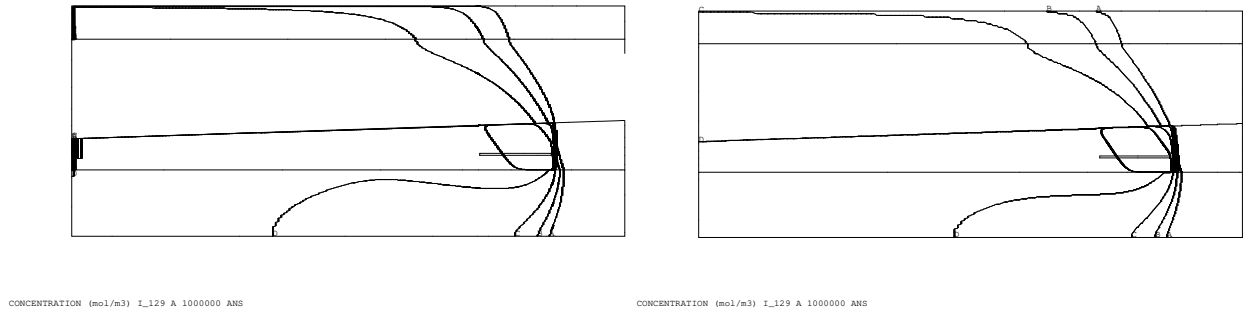

Figure 12. Results at 1000000 years, grid GQ5 - quadrangles - with an FE discretization (left) and grid GR4 - rectangles - with an MHFE discretization (right)

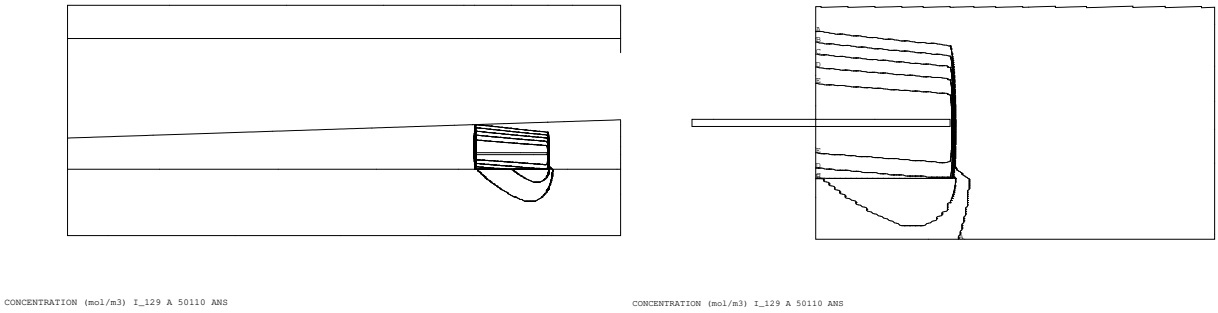

Figure 13. Results at 50110 years, grids GQ5 - quadrangles, FE discretization

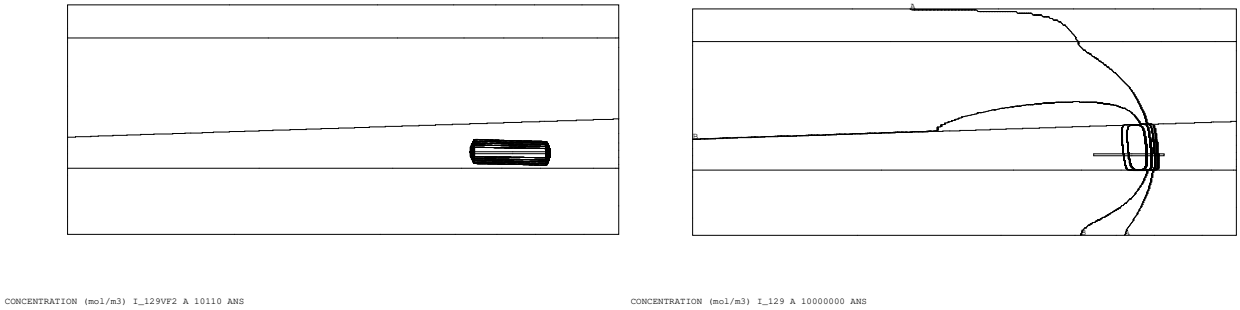

Figure 14. Results at 10110 years, grid GQ2 with an FV discretization (left) and at 10 million years, grid GR4 - rectangles with an MHFE discretization (right)

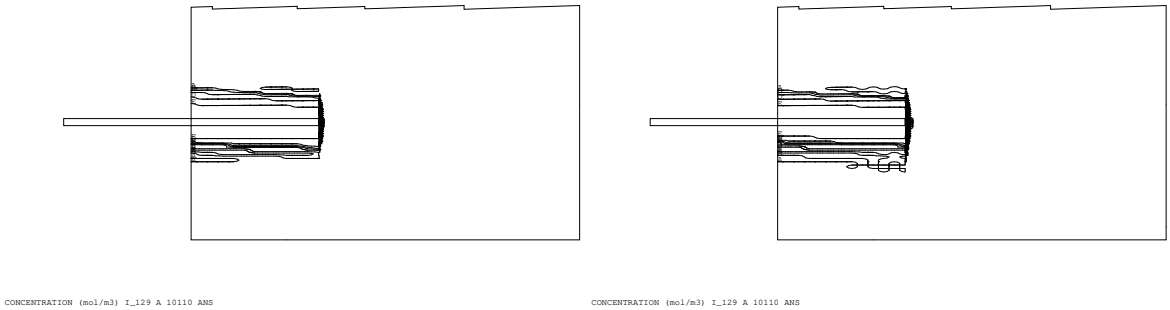

Figure 15. Oscillations of the concentration 10110 years, grids GQ2 - quadrangles, FE discretization (left) and MHFE discretization (right), no mass lumping

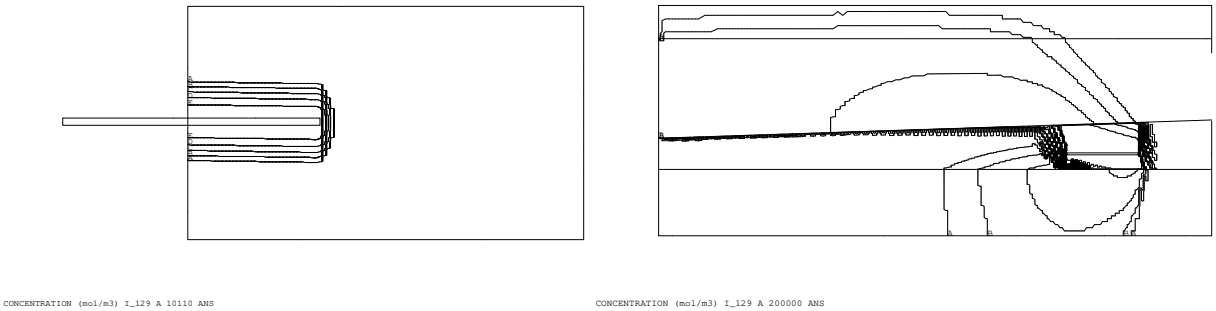

Figure 16. grids GQ2, results at 10110 years, MHFE discretization (left) and at 200000 years, FE discretization (right), with mass lumping techniques, centered convective terms